Fabrication of Mass Produced Microdot Arrays for use as Micro-Targets on High-Repetition Rate Experiments.

Contact *Graham.Arthur@ScitechPrecision.com*

Graham Arthur
Scitech Precision Ltd., Rutherford Appleton Laboratory, Harwell Oxford, Didcot, OX11 0QX, UK

C. Spindloe
Central Laser Facility, Rutherford Appleton Laboratory, Science and Technology Facilities Council, Harwell Oxford, Didcot, Oxon, OX11 0QX

Introduction

High Power Laser experiments to carry out fundamental research on subjects such as ion acceleration or condensed matter studies may require microdot targets of materials such as aluminium and iron. For example, when irradiating solid samples with the output of a free electron laser x-ray source the intensity distribution on target in such setups can span many orders of magnitude. As pulse shaping capabilities are not currently available in the X-ray regime one solution to this problem is to use dot targets which are smaller than the focused beam and thus spatially limit the range of intensities incident on the target. Typically these microdots are 3 to 5 microns in diameter with thicknesses up to a few microns, depending upon the material used. Furthermore, these dots need to be suspended by a minimal amount of low-Z support material and not simply mounted on the surface of a thick substrate. With the development of high repetition rate laser systems these microdots are shot in rapid succession (~1 min) and therefore the experiment requires a large number of such dots on a well defined grid to aid locating and rapidly stepping between dots during the experimental run.

In the example described below, Fe microdot targets of 5 microns diameter were suspended on 1 micron thick CH film which spans an array of cavities in the substrate. These cavities were 350 microns in diameter in array sizes of 40 x 40 giving 1600 targets in an area of approximately 25mm x 25mm. To aid the experimenter, alignment arrows were also placed on the substrate at the corners of the array. These are patterned at the same time as the dot array and are therefore precisely located with respect to the dots.

This paper will describe the fabrication of such microdot target arrays and will discuss the MEMS-based microfabrication processes involved and how they might need to be modified compared to standard semiconductor fabrication processes to take into account the materials and how they are to be used.

Fabrication Techniques

Manufacture of laser targets with these dimensions and in the quantities required, requires a different approach to those usually seen in laser target fabrication. The micro-electro-mechanical system (MEMS) fabrication technologies developed from the semiconductor manufacturing industry offers the opportunity to fabricate such targets.

These technologies are based upon three basic techniques: deposition, patterning and etching and are described briefly below.

1. Deposition

This includes sputter-coating, thermal evaporation, chemical vapour deposition, thermal oxide growth and spin/dip coating. Thus it is possible to deposit precisely controlled films of metals, dielectrics and polymers.

2. Etching

This may be either dry etching or wet etching. In the former plasma containing highly reactive species (e.g. fluorine, chlorine) is generated and this etches the substrate and/or previously deposited thin films. In the latter, the substrate and its coatings are immersed in a solution which is selected to etch the required layer.

3. Patterning

This is the key process and uses either optical tools or e-beams to pattern a thin film of photo, or e-beam sensitive resist applied to the substrate by spin/dip coating. The patterned resist film is then used as a protective stencil through which deposition or etching can take place, thereby transferring the pattern into the substrate or its coatings.

Optical lithography uses photomasks to define the patterns. These usually comprise of an extremely flat quartz plate with the pattern defined on one side of that plate in a 100nm layer of chromium. In cases where only low resolution is required a photomask defined on an acetate sheet by high resolution inkjet printing may be used to reduce costs, but are prone to greater wear and tear with repeated use and can suffer from excessive thermal expansion in poorly controlled processing environments.

A technique known as lift-off is essential for the fabrication of the microdot targets and is a combination of deposition by thermal evaporation and patterning using a bilayer film of resist. It allows the dots to be deposited with precise dimensions and with cleanly defined edges.

Special Precautions

MEMS fabrication techniques were originally developed from semiconductor manufacturing process and both industries use a rather more limited number of materials than laser targets may require. For example laser targets may be made from gold, iron, aluminium, copper, samarium, titanium, bismuth, yttrium, lithium, boron, various polymers etc. Therefore it is important that the fabrication processes are compatible with these materials. For example, during the work reported here, standard gold etch solution was found to attack iron coatings and so it was necessary to include an additional coating step to protect the iron dots from the gold etching towards the end of the manufacturing process.

Device Fabrication

Initial steps

The chosen substrates for the Fe dot target arrays were 100mm silicon wafers of 325 microns thickness. Patterning used only optical lithography and, by a combination of wafer inversions and photomask rotations, it was possible to incorporate all the required process steps onto a single quartz photomask. The CAD design and photomask are shown in Figure 1.

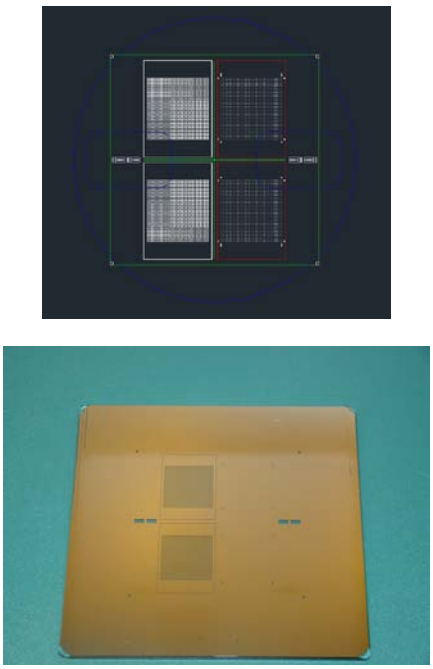

Figure 1. CAD design for the Fe dot target photomask *(top)* and photograph of the finished photomask *(bottom)*.

It would be very difficult to identify the iron alignment marks on a polished Si wafer and therefore the first process step was to coat the front face of the wafers with gold, thereby providing good optical contrast between the Fe alignment marks and the substrate. Following this, the 1 micron parylene support film was deposited onto the Au. Thick metal depositions are prone to developing stress as the layer thickness increases and can delaminate when subjected to mechanical or thermal shock. Therefore, the parylene film was then coated with a 5nm Fe film which would act as an adhesion layer between the parylene and thick Fe dot. A coating of only 5nm was chosen so not to interfere with the experimental results.

Lift-off process

The next process steps are the most critical as they define the dimensions and edge roughness of the dot targets. For this a bilayer resist was used for the Fe lift-off process. The two resist layers are chosen such that after patterning the lower layer undercuts the top layer, giving an overhanging resist profile (Figure 2). This is done so that when the Fe is deposited, it is does not form a continuous film over the resist and simple immersion in a suitable solvent, lifts off the unwanted Fe, leaving only the dot structures, with cleanly defined edges (Figures 3 & 4).

Figure 2. Overhanging resist profile on substrate.

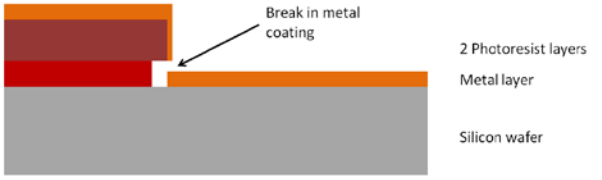

Figure 3. Thermal evaporation of iron.

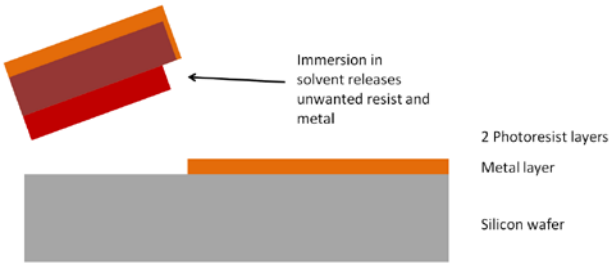

Figure 4. Iron lift-off in solvent.

Following the lift-off process, the wafer is prepared for further lithography and dry etching on the underside. This etching process simultaneously etches away the substrate underneath the Fe dots, creating the 350 micron cavities, and dices the substrate into the final 25mm x 23mm rectangles. The final step, before mounting, was to remove the gold coating underneath the parylene in the etched cavities.

Results

The finished target arrays are shown in the Figures 5 to 7. Figure 5 shows the silicon target support structure with the 350 micron diameter cavities in a 4 x 40 array. Figure 6 shows an optical close-up of four such cavities. The Fe dots can just be discerned in the centre of each cavity. Figure 7 shows an SEM image of one of the Fe dots. In this case the diameter is 5 microns and the dot thickness is approximately 1 micron.

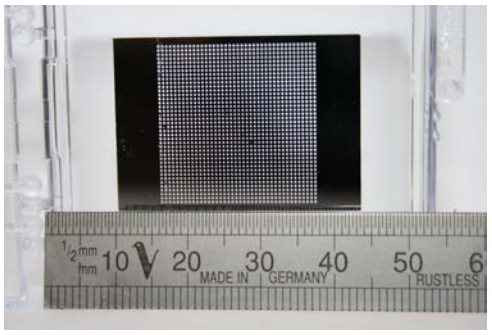

Figure 5. Dry etched silicon support structure for a 40 x 40 array of Fe dot targets.

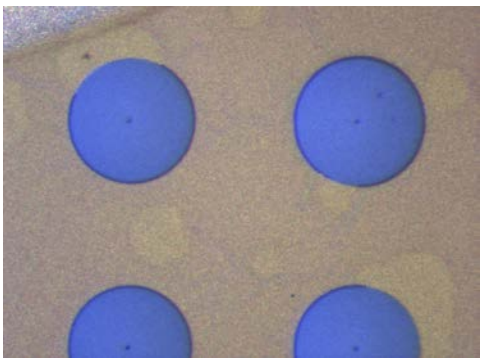

Figure 6. Optical close-up of four of the 350 micron cavities. The Fe dots can just be discerned.

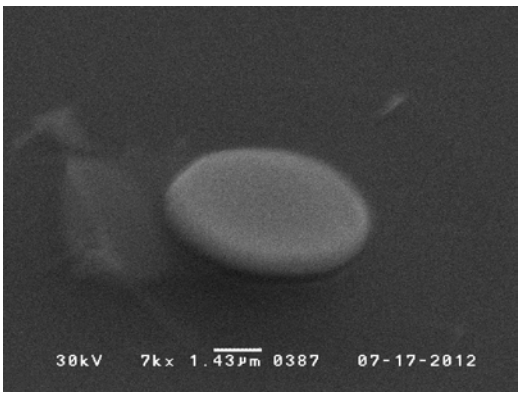

Figure 7. SEM image of a typical Fe dot target viewed at an angle of approximately 50 degrees. The dot diameter is 5 microns and its thickness is approximately 1 micron.

Conclusions

Figure 7 demonstrates that iron microdot targets can be fabricated using the described procedure and an initial batch of two 40 x 40 arrays was produced and shipped to LCLS for an experimental run. At the time of writing, the results are still awaited.

Microdot yield in this initial batch was lower than anticipated but after close examination of the process steps the procedure has been modified and it is hoped that the future runs will result in a higher yield.

Thin-film measurements of multilayered foils using Electron Dispersive X-ray spectroscopy.

Contact *Frank.Hall@ScitechPrecision.com*

Frank Hall
Scitech Precision Limited,
Rutherford Appleton Laboratory,
Harwell Science and Innovation Campus,
Didcot, Oxfordshire, OX11 0QX

Chris Spindloe, M. K. Tolley
Target Fabrication, Central Laser Facility,
Rutherford Appleton Laboratory,
Science and Technology Facilities Council
Harwell, Didcot, OX11 0QX

Introduction

There are a wide variety of uses for thin film coatings and multilayered thin foils including optical coatings, phase plates, x-ray backlighters, filters, etc. What is essential is that the thickness of these deposited layers is known but in some cases traditional thickness measurements are not suitable or appropriate. A non-destructive method for making such measurements is described.

Multi-material, multi-layered thin foils were produced for an experiment to be used as x-ray backlighters for nanosecond time-resolved Laue diffraction to study dynamic processes in condensed matter physics[1]. These foils have been produced using evaporative techniques and some of the difficulties in producing them are outlined.

The technique involves using a scanning electron microscope to probe a sample. As the beam energy is increased the penetration depth of the electrons increases. When the energy is high enough the electrons will pass through the coated layer and into the substrate and will at this point begin to give out a characteristic x-ray signal.

Deposition

Several methods are available for depositing materials that are more or less suitable depending on the material. Given the vacuum level that the coating plants can get down to some materials will evaporate and some will sublime. Other factors to consider are the form that the evaporant takes (pellets, powder), whether an oxide layer exists, coating rate, substrate and system geometry.

In thermal deposition a current is passed through a coil which generates heat. The evaporant is placed within the coil and as the temperature rises the evaporant vapour pressure increases significantly and coating begins. A number of coil designs are available and alter the nature of how the sample is heated.

In electron beam deposition the heating of the substrate comes from an incident beam of electrons. The evaporant is held within a crucible and heating comes from above. The electron beam sweeps in a raster fashion providing heat distribution across the surface of the evaporant. This is useful for a material that needs to be 'run in':- pre-heated to outgas, remove oxide layers, melt, etc.

Sputter coating uses an inert gas (typically argon) to bombard the source material, scattering material off to be coated. The higher gas pressure acts as a moderator to the ejected material allowing a random walk before coating which typically eliminates shadowing and can be useful in certain situations.

Current thickness measurements

When a component is to be coated, a glass slide is also put into the coating chamber and is used sacrificially to test thickness. A scratch is made in the coating on the glass slide and a linear surface profiler is used to examine the depth of the trench.

The downside of such a measurement is that the true thickness of the coating on the component may be slightly different to that on the slide due to a difference in sticking coefficients, re-sputtering, chamber geometry, etc. To illustrate this point, a slide was coated with silver (Ag) and this was destructively measured at one point on the slide as 100nm. This was then coated a second time along with a new slide, again with silver. The new slide had a thickness of 100nm but the original slide, measured at a new position, had a thickness of 210nm. However, destructively testing the component is not often a viable option.

Electron Dispersive X-Ray Spectroscopy

A standard electron microscope fitted with an Electron Dispersive X-ray (EDX) Spectrometer can used to perform the elemental analysis of samples. Each element has a characteristic set of x-ray emission lines which can be used to identify it within a sample. The incident beam of electrons must have more energy than the emission line in order for it to be observed. As an example chlorine has a Ka_1 emission line at 2.622 keV and so to test for the presence of chlorine a beam energy of around 3keV or greater would be required. The user can set the beam energy, which determines the size of the volume within the sample being examined, and more specifically for thickness measurements, the maximum penetration depth. This is known as the Bethe range, discussed later. For the experiment the following energies were available: 1, 2, 3, 4, 5, 6, 7, 8, 9, 10, 15, 20, 25 and 30keV.

Bethe Range and Theory

Kanaya and Okayama[2] collated many texts both theoretical and experimental on electron interactions with solid matter related specifically to Scanning Electron Microscopy. Within their work which covered transmission and backscatter of electrons, energy absorption through elastic and inelastic collisions as well as modeling, they derived the maximum penetration depth of an incident beam of electrons, otherwise known as the Bethe Range,

$$R(nm) = \frac{27.6AE_0^{5/3}}{\rho Z^{8/9}} \quad (1)$$

where A (g) is the atomic weight; E_0 (keV) is the beam energy; ρ (g/cm^3) is the density; and Z is the atomic number.

For the purpose of thin-film measurements the equation relates a beam energy to a maximum depth taking into account the properties of the transmitting material. However it does not account for measurements to be taken from within a substrate

via x-ray emission and the associated energies when examining components nor for examining multilayered materials.

When the Bethe Range is greater than the thickness of the coated layer then incident electrons begin to enter the substrate but do not necessarily possess enough energy to generate the substrate's characteristic x-rays. It is therefore proposed that in order to 'observe' the substrate a total beam energy, E_T, is required such that:

$$E_T^{5/3} = E_\lambda^{5/3} + E_1^{5/3} + E_2^{5/3} + \ldots + E_n^{5/3} \qquad (2)$$

where E_λ is the characteristic x-ray emission energy for the substrate and $E_{1,2,\ldots n}$ are the energies required to penetrate each coated layer separately. In principle, since this is the minimum energy required to 'observe' the substrate the corresponding peak would be lost in the Bremsstrahlung, however taking higher energy readings would allow one to backtrack to this point as will be explained next. This minimum energy is known as the *zero point* of emission.

Methodology

A series of aluminium test runs of varying thickness were performed for simplicity to check against theoretical predictions before examining a dual-material dual-coating Caesium Iodide (CsI) / Tin Telluride (SnTe) / Glass substrate sample.

A series of spectra were obtained for each sample while varying the beam energy using the energies outlined previously. For each spectrum the background Bremsstrahlung was automatically removed via software and the resulting peak heights were recorded for the coating materials and substrate. These heights were then normalized since the peak height is governed by the system alignment whereas the relative peak heights holds the information on the sample composition.

Each spectra was obtained with 200,000 x-ray counts in an attempt to create consistency between scans. The samples were mounted at 35° to increase the x-ray signal (see fig 1). This of course changes the geometry for calculating sample thicknesses. For simplicity each sample thickness was recorded as the length vertically straight down to the substrate via standard trigonometry. From now on the increased value is that shown. A total of 5 Al thicknesses were tested: 61nm, 107nm, 206nm, 366nm and 781nm measured previously via a touch-probe linear profiler.

Results

Looking at a typical Al coating, here 88nm we can calculate the vertical distance to the substrate given a sample angle of 35° as 88nm/cos(35°) = 107nm. Using this as the Bethe Range it is possible to calculate the required beam energy, E_0, via equation 1, in this case 2.23keV. Fig 2 shows a simulation of the electron beam penetrating into the Al coating and only just managing to reach the substrate based on this energy. If we then add in the energy required to observe the Si (1.74keV) substrate, E_λ, then the total energy, E_T, becomes 3.02keV via equation 2. This can then be compared with fig 3.

Measurements beyond 3keV are performed to aid in backtracking to the point where the Si peak is zero: the zero point. Problems can occur in identifying the zero point if the Bremsstrahlung is not removed correctly and, as will be seen later, where insufficient data points are available. The data for each of the 5 Al samples can be found in table 1 where the calculated and observed values match to within ±0.1 keV.

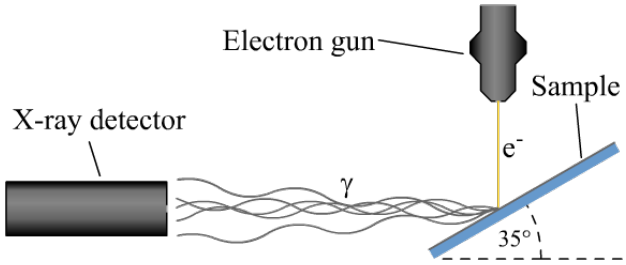

Figure 1 - shows the alignment of the sample within the SEM.

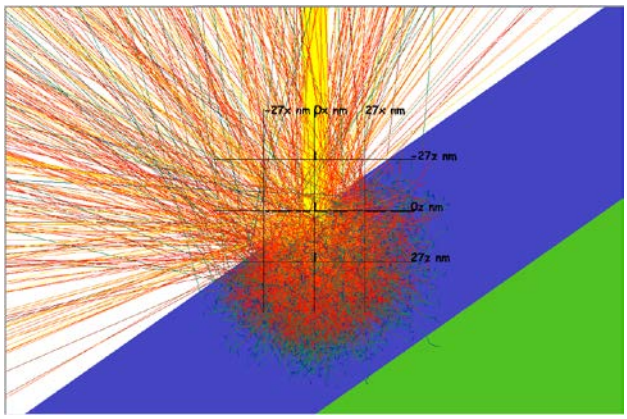

Figure 2 – Simulation[3] of penetrating electron beam into an 88nm thick Al layer (blue) on a SiO_2 substrate at 35°. The colour of the electron trails depicts their energy.

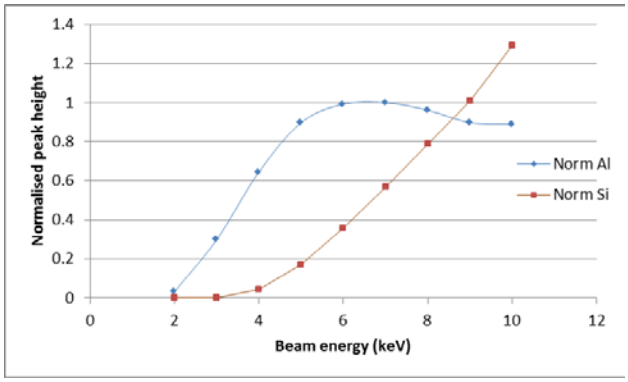

Figure 3 - Peak heights for Al (107nm) and Si (SiO_2 substrate) for beam energies from 2 - 10keV.

Al known thickness (nm)	Substrate material & emission (keV)	Calculated total energy (keV)	Measured substrate zero point (keV)
61	Na 1.04	2.02	1.9
107	Si 1.74	3.02	3.0
206	Si 1.74	3.94	3.8
366	Si 1.74	5.18	5.2
781	Si 1.74	7.74	7.7

Table 1 - Shows the calculated and measured zero points for 5 Al samples of various thicknesses.

Spectra of the dual-material dual-coating CsI / SnTe / Glass substrate can be seen in fig 4 for energies between 2 – 20keV. It shows graphically how the peaks from the various materials become visible at increasing energies. For Si strong peaks can only be seen at 15 and 20keV, potentially hindering the ability to determine the zero point.

Looking specifically at the 3.4 – 4.3keV emission lines for Cs, I, Sn and Te, and for Si at 1.74keV, the heights of these peaks can be seen in fig 5. A zoomed in version can be seen in fig 6 and from this the point of zero emission is to be obtained. Clearly there is some difficulty in accurately identifying this energy both for SnTe and especially for Si. When removing the Bremsstrahlung the software looks for a line running through the center of a region of white noise and can erroneously generate peaks (Sn peaks in fig 7).

Clearly equal proportions of the spectrum lie above and below the line of Bremsstrahlung and as such the peaks shown here should be, at the least, smaller. Looking for peaks amongst the Bremsstrahlung is the cause for the persistent readings of Si between 4 and 9 keV (fig 5).

Each element has its own x-ray emission energies and so the zero point for each is calculated separately despite the coatings appearing in the layers in pairs. For the upper most layer, (CsI), the zero point should be equal to the x-ray emission energy. Where integer beam energies were used and plotted, decimal values are extrapolated. The findings are found in table 2.

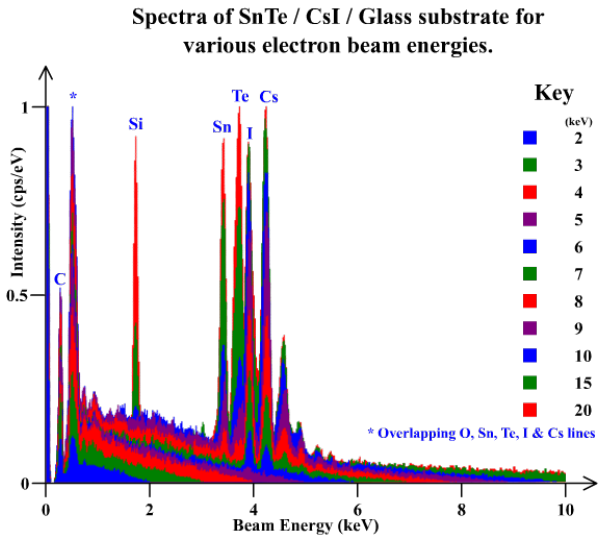

Figure 4 - Spectra for increasing beam energies for a 331nm CsI / 365nm SnTe / Glass substrate sample.

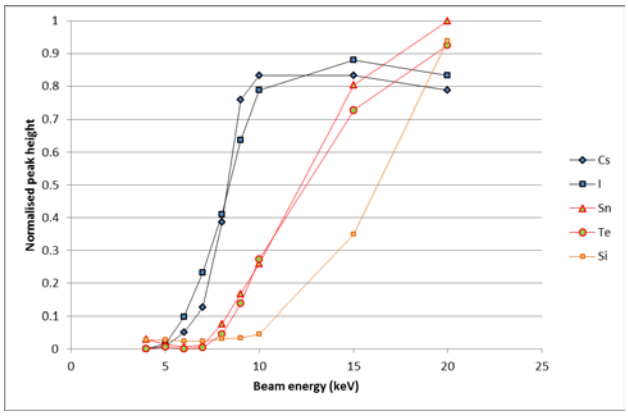

Figure 5 - Normalised peak heights as of fig 4.

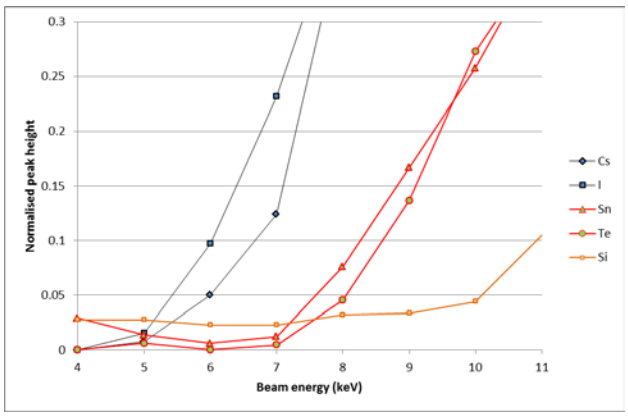

Figure 6 - Close up of fig 5 used to determine the zero points for SnTe and Si.

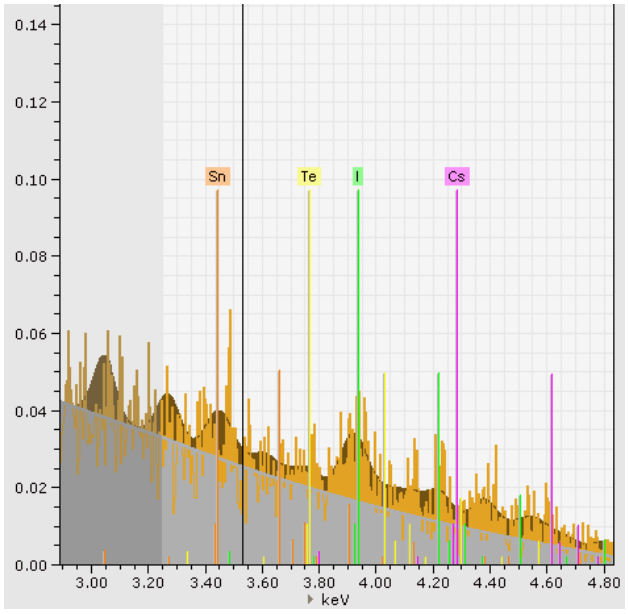

Figure 7 - Erroneous peaks generated by the software (far left for Sn).

	Emission line (keV)	Measured zero point (keV)	Zero point inferred thickness (nm)	Actual thickness of above coating
Cs	4.29	4.5	-	N/A
I	3.94	4.0	-	N/A
Sn	3.44	6.3	313	331
Te	3.77	6.8	350	331
Si	1.74	9.0	352	365

Table 2 - Shows the calculated and actual thicnesses of the coated layers CsI and SnTe.

Clearly there is a greater degree of error in assessing the zero point of emissions than was apparent with the Al test samples. However given the increased complexity of measuring the double layered multi-material coating, the calculated thicknesses fall within a 10% margin. The zero point for cesium and iodine is measured close to the value of the emission line. The values of the inferred thickness from tin and tellurium are expected to be the same but a small variation is seen here. The

average does however match the expected thickness very well (331.5nm). This value was used with the Si zero point to calculate the thickness of the SnTe layer. It is in fairly good agreement with the actual value.

Discussion

This technique is suitable as a method for non-destructively measuring the thicknesses of multi-layer coatings or foils. However the technique could be enhanced to increase the accuracy of measurements. Firstly, an improved SEM with 0.1keV beam energy increments or finer would vastly improve resolution and could be delivered only at energies around the zero points so as to limit the increase in scan times. Increasing the number of counts would flatten out the Bremsstrahlung at the cost of scan time but would be suitable for energies above 10keV where the count rate is high. Work could also be done to mathematically calculate the zero point from the higher energy data points where the x-ray signal is much stronger against the background Bremsstrahlung.

Simulations

Target Fabrication has access to software that can model the electron beam parameters such as beam energy, beam size, sweep and shape, and can incorporate nearly any shape and size of sample and of course multiple layers.

This powerful tool can save time in determining the beam energy required to penetrate a given layer and also gives a wide range of data including backscattered angle & energy, Z_{max}, energy by position etc which are not included in this report.

Conclusions

In its current state non-destructive thin-film measurements can be performed using SEM EDX spectroscopy to an accuracy of approximately 10% for single or multiple layers with a total thickness up to about 2 microns depending on the materials.

References

1. Suggit, M. et al, 2010, Nanosecond x-ray Laue diffraction apparatus suitable for laser shock compression experiments, Review of Scientific Instruments 81(8)
2. Kanaya, K. and Okayama S., 1972, Penetration and energy-loss theory of electrons in solid targets, J. Phys. D: Appl. Phys., Vol. 5
3. CASINO Monte Carlo simulation software, Drouin, D. et al, © 2011, Universite de Sherbrooke, Sherbrooke, Quebec, Canada.

High Volume Production of Thin Foil Laser Targets for Use on Next Generation Laser Facilities

Contact *christopher.spindloe@stfc.ac.uk*

C. Spindloe, S. Tomlinson, M.K. Tolley

Central Laser Facility, Rutherford Appleton Laboratory, Science and Technology Facilities Council, Harwell Oxford, Didcot, Oxon, OX11 0QX,

G. Arthur

Scitech Precision Ltd, Rutherford Appleton Laboratory, Harwell Oxford, Didcot, Oxon, OX11 0QX.

S. Astbury

York Plasma Institute, Department of Physics, University of York, Heslington, York. YO10 5DD,

Introduction

There is development across Europe and the wider international community of high power high repetition rate laser systems such as the Astra Gemini laser at RAL [1] the ELI project [2] and eventually IFE facilities such as HiPER [3] and LIFE [4]. Established methods of target fabrication are less suited to meeting the high volume demand for high specification targets. This demand coupled with the developing application based platform for laser sources, as demonstrated by the recent Libra [5] project, has created a need for a source of laser targets that is reproducible and also flexible around a common insertion mechanism. This report looks at the Central Laser Facility development project to produce a 'Nano-positioning wheel' concept and to develop the target technologies required to deliver a reliable high production number stream of targets to this wheel.

Experimental Delivery

It is first essential to consider the applications that are to be covered by this development. While it is possible to deliver a wheel based system to field laser targets [6] these capabilities are usually limited to a low number of target types. They are also are limited by target number for the most interesting of target types. For example, it is possible to purchase ~10 micron thick foils of a variety of different materials and to develop a simple array mount to field targets of up to 1000 per cartridge for a simple experiment. However, as has been discovered using the Astra Gemini laser at RAL experiments usually require significantly more sophisticated targets. While a number of groups have produced systems that are suitable for one type of target and experiment this project aims to deliver a robust solution to a wide range of experimental and (eventually) application based targets.

The wide variety of targets required for an experiment are often 1) orders of magnitude thinner than purchased foils and approaching 1-5 nanometer thickness, 2) complex multi-layer targets that are not commercially available, 3) varying across the experiment requiring up to 10-20 types of geometry, material and in some cases requiring a number of different mounting techniques to be able to field the target. To date these requirements have not been fully delivered on an experimental scale.

In addition to the above three considerations it is essential to take into account the challenges of delivering complex geometries such as multi target clusters, 3D micro-machined targets and multi element (both mechanical and chemical element) targets that require a number of assembly steps.

The RAL system has been engineered to integrate the recent developments in using MEMS (Micro Electro-Mechanical Systems) to deliver targets that would have not previously been achievable. Targets such as SiN spoke targets [7] have been produced at RAL in large numbers; indent micro cone targets [8] and also micro-dots supported on thin membranes [9] have also been produced. While these represent the cutting edge of 2 and 2.5 dimensional targets the technology can be used to produce significantly simpler targets in the first instance.

Nano-positioning Wheel

A system has been designed at RAL to field targets that are produced around the outside of a 100 or 150mm diameter wafer. The populated disk is mounted on a stage that has 6 axis controls (3 linear and 3 rotational stages). These stages can move independently allowing the wheel to be incremented around while enabling an individual target to be precisely moved to a defined target position.

Each motion control stage is fitted with a 5nm resolution Renishaw encoder to enable accurate and measured positioning of the stage within the vacuum chamber during experiments, preventing the need to let up the chamber to deal with alignment issues. A schematic diagram of the stage and mounted disk is shown in figure 1.

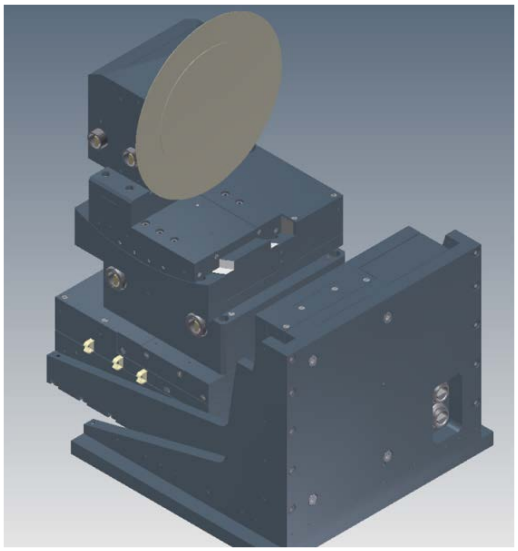

Figure 1: A schematic representation of the stage holding a 150mm diameter wafer patterned with a number of targets.

It is essential that at least 1000+ targets can be fielded onto a target wheel to take advantage of the high repetition rate of the latest generation lasers and also to make the wheel experimentally relevant. Some other target delivery solutions for individual research groups can deliver similar numbers for single target types and the wheel needs to deliver these numbers and allow for the flexibility that is inherently needed in experiments and is not currently achievable on high rep rate laser systems.

Material Trials

The first fabrication tests were carried out using a 100mm diameter silicon wafer, patterned with a number of holes. These holes were produced using conventional MEMS techniques combined with well known thin film coating techniques. A silicon wafer was coated with 5um Parylene (CH 'N') on one side. The reverse was then patterned using a standard resist, exposed to UV light and then developed to produce a mask on the rear. The sample was then placed in a Deep Reactive Ion Etcher (DRIE) to remove the silicon where it was exposed and etched though to the Parylene membrane.

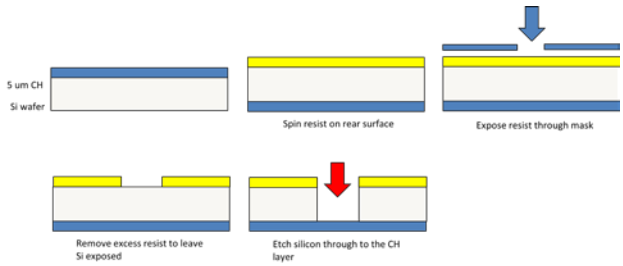

Figure 2: The etching process for producing the target membranes

The produced Parylene membranes were extremely flat and there was a 100% yield. A scan of the surface of one of the membranes is shown in figure 3. From the scan it can be seen that the foil takes on the structure of the wafer that it was coated onto. In this case the Parylene was coated onto the rear of the wafer which was unpolished and so there is some inherent roughness in the foil of ~150nm. The roughness can be eliminated by using the polished side or double side polished wafers.

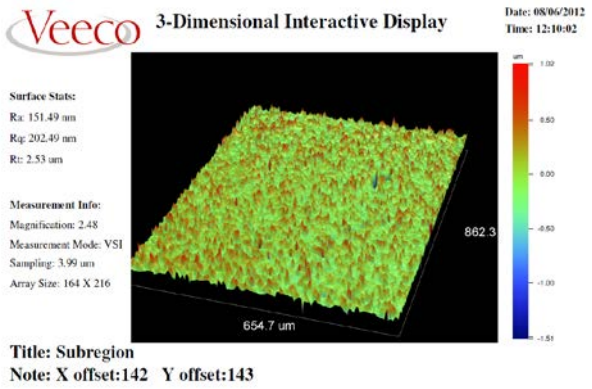

Figure 3: A surface scan of a thin Parylene membrane

Optical images of the wafer are shown in figures 4a and 4b. While encouraging the result is for a thick (5µm) foil and the techniques need to be demonstrated for much thinner membranes. Work is ongoing to produce membranes that are sub -um thick and to work with a number of different materials and geometries.

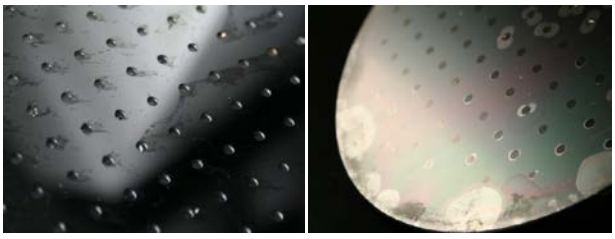

Figure 4a and 4b: An image of the rear (left) and front (right) of a disk after etching.

Initial Trials - Geometry

In addition to carrying out etch tests for Parylene other work was carried out to produce the exact wafer geometry that was required for attachment to the stage. A photo mask was produced that had 3 concentric rings of target holes around the outside and also had patterned the holes that would be required for fixing to the chuck of the stage. A 100mm diameter wafer was used. It was coated with a number of layers for processing including a thin SiN 'target' layer and was processed using conventional UV lithography. The results of this can be seen in figure 5.

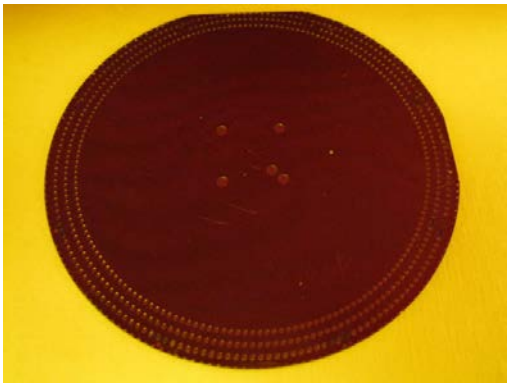

Figure 5: a processed silicon wafer with 3 concentric rings of targets patterned at the edge.

From these initial trails and in response to the need for more flexibility in the targets that can be supplied to the wheel it was decided to produce a separate target holding ring and then produce smaller sections of silicon wafer containing the targets. The sections can be produced with different materials, thicknesses or even geometries and then placed on the ring with up to eight different sections able to be mounted on one ring. The design in figure 6 shows the schematic for this.

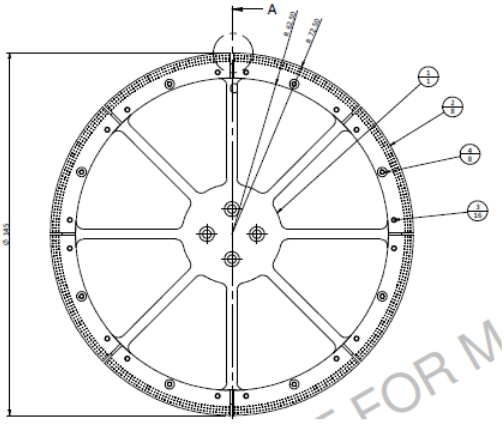

Figure 6 Design for the target holding ring

An initial test was carried out to produce the wheel sections. Using a silicon wafer coated with a number of masking and protection layers as well as a 5um CH coating it was possible to etch the target components and produce individual wheel sections. The techniques described earlier were used to deposit the layers and also to etch through the silicon. The polished side of a wafer was used as the coated face to improve the surface roughness from the earlier tests. The etching also included the provision of holes for mounting on the frames shown in figure 6. A picture of the wheel sections is shown in figure 7.

Figure 7: A single wheel section with target holes and mounting features

As detailed earlier the surface roughness of the foils produced in the trials was of the order of 180nm. Characterisation of the new wheel sections using white light interferometry and also using confocal microscopy shows that the surface roughness is much reduced to a few nm. Figure 8 shows a surface scan of a ~50 micron area of the foil, which is comparable to the laser focal spot and therefore is a good representation of the roughness that the laser will see. This value of ~2nm is comparable to the surface roughness of foils that are produced using the standard method of coating onto slides and floating off onto mounts.

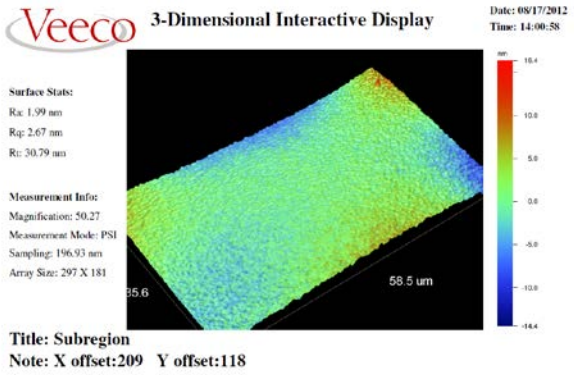

Figure 8: Surface roughness of the wheel section for the nano-wheel (50 micron area)

Conclusions

Further work is required to establish production techniques. Films thinner than currently produced are required and testing is needed to ensure that the wheel can deliver the targets to the interaction point with high accuracy. Investigation is required into the mechanisms of shock damage to nearest neighbour targets and to determine the optimum layout of the targets on the wafer. Following this it is essential to develop more complex targetry streams for the stage. However initial trials have shown that simple thin foil targets can be produced in high numbers and the nano-positioning wheel concept has the ability to be a flexible method of delivering these targets to an experiment.

Acknowledgements

The author would like to thank S. Serra and E. Barber for their work on the initial target tests and the previous MEMS targets produced at RAL.

References

1. The Astra Gemini Project – A dual-beam petawatt Ti:Sapphire laser system. C.J. HOOKER, J.L. COLLIER, O. CHEKHLOV, R. CLARKE, E. DIVALL, K. ERTEL, B. FELL, P. FOSTER, S. HANCOCK, A. LANGLEY, D. NEELY, J. SMITH AND B. WYBORN. **J. Phys. IV France. 133, 673-677 (2006).**
2. http://www.extreme-light-infrastructure.eu/
3. http://www.hiper-laser.org/
4. https://life.llnl.gov/
5. http://www.qub.ac.uk/sites/LIBRA/
6. High repetition rate microtarget delivery to the Astra Gemini laser. C. SPINDLOE, M. K. TOLLEY AND E. DIVALL G. SCHAUMANN W. NAZAROV. **CLF Annual Report 2080-2009**
7. Production of multi-MeV per nucleon ions in the controlled amount of matter mode (CAM) by using causally isolated targets. STRANGIO C., CARUSO A., NEELY D., ANDREOLI, P.L., ANZALONE R., CLARKE R.,CRISTOFARI G., DEL PRETE E., DI GIORGIO G., MURPHY C., RICCI C., STEVENS R., TOLLEY M., **Laser and Particle Beams, 25, 1–7 (2007).**
8. Novel Micro-Focusing Cone Target Fabrication C.SPINDLOE, G.SCOTT, S.SERRA AND DAVID NEELY. **CLF Annual Report 2010-2011**
9. Fabrication of Mass Produced Microdot Arrays for use as Micro-Targets on High-Repetition Rate Experiments. G.ARTHUR. **CLF Annual Report 2011-2012**

Design for Production of Thin Film Solid Hydrogen Targets

Contact *steph.tomlinson@stfc.ac.uk*

Stephanie Tomlinson, Chris Spindloe, Paul Holligan and Martin Tolley

Central Laser Facility, Rutherford Appleton Laboratory, Science and Technology Facilities Council, Harwell Oxford, Didcot, Oxon, OX11 0QX,

Introduction

There is interest in accessing new physical mechanisms for the acceleration of ions using high energy lasers, one of which is Light Sail Radiation Pressure Acceleration (LSRPA). The efficiency and maximum energy achievable scales favourably when the density of the material is decreased. LSRPA requires a solid thin film target and the material with the lowest solid density is hydrogen. Therefore there is the need to develop windowless thin film solid hydrogen targets for monoprotonic hydrogen, deuterium and mixtures of both isotopes.

CLF is currently developing a cryogenic system to produce solid hydrogen targets using a condensation method. The desired target parameters are 2-5mm diameter and 50 micron thickness. The target and cryogenic system will be situated in a vacuum of $1x10^{-6}$mbar within a target chamber required for laser operations.

Background and Approach

There has been interest in the field of solid hydrogen targets for the development of laser fusion. Windowless hydrogen targets have been successfully produced before using 3 methods; extrusion[1], casting[2] and condensation[3]. However, the dimensional parameters of the targets produced previously do not match the thin film parameters required for LSRPA.

Cylindrical extruded targets were produced successfully (figure 1) but it would be difficult to produce thin films using the extrusion method because of anisotropic die swell, which would lead to the targets curling. Alignment of the laser relative to the extruded target would also prove a challenge. The casting method was successful for producing targets of 5-10mm thickness (figure 2), but there was concern that a thin film target would tear when the casting plates were removed. Allowing a thick target to evaporate to a thin film target was considered, but it would be difficult to control the target parameters reliably.

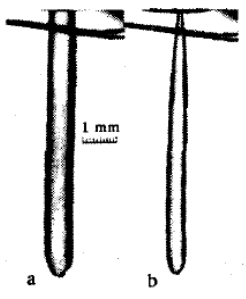

Figure 1: Extruded Target[1]

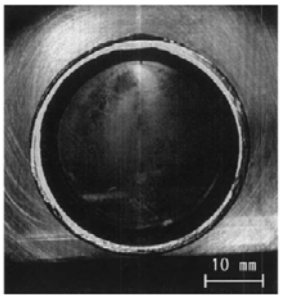

Figure 2: Cast Target[2]

The method deemed most likely to produce the thin film targets successfully and reliably was the condensation method in which liquid hydrogen is condensed onto a target substrate.

Hydrogen Properties

The properties of hydrogen and its phase behavior define what cooling and control methods are required for the design of the cryogenic targetry system.

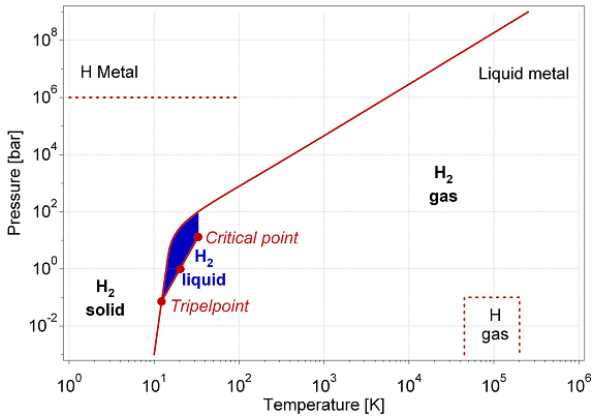

Figure 3: Phase Diagram for Hydrogen[4]

The condensation method requires hydrogen to be in a state where a wet vapour is produced, so that the gas will condense onto a plate to create a liquid film which flows over the target hole. The next stage is to change the phase of the thin film from liquid to solid. The phase state is dependent upon the temperature and pressure. During the condensation phase, the pressure needs to be kept constant while the temperature is lowered, so that the hydrogen is in the blue region shown in figure 3. It is important to stay above the triple point, as sudden changes in density must be avoided. Therefore the design of the system needs to control the temperature and pressure of the hydrogen such that it is kept between the critical and triple point.

	Hydrogen	Deuterium
Pressure at Critical Point (bar)	**13**	**16.6**
Temperature at Critical Point (K)	**33.5**	**38.4**
Pressure at Triple Point (bar)	**0.07**	**0.17**
Temperature at Triple Point (K)	**13.8**	**18.7**

Figure 4: Triple point and Critical Point Data

A decrease in temperature shall then solidify the hydrogen, at which point the local pressure boundary can be removed and target exposed to vacuum pressures.

Mechanical Design

A 4K Pulse Tube Cryocooler is utilised to cool the target end. The pulse tube was selected over other cryo cooling options as it provides low vibration, which is essential for laser applications. A target mount is fixed to the end of the pulse tube to hold the target foils, provide a large conductive mass to reduce large temperature gradients during temperature control and provide a suitable location for heaters and temperature sensors (figures 5 & 6). The pulse tube does not have temperature control, so heaters and sensors are used to control the temperature of the target mount.

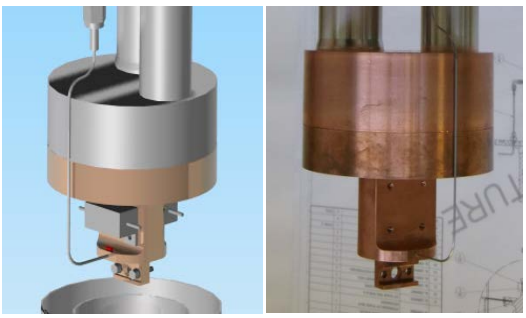

Figure 5 & 6 Target Mount

The target foil needs to be kept in a constant pressure of hydrogen to allow the gas to condense onto the foil. The whole system is in a vacuum chamber, so a local removable gas boundary is used to contain a small volume of gas around the foil during target production. A clear PMMA boundary is used and supported on a linear translation stage using a low conductivity connection tube. A pressure sensor is fitted to the local boundary (figure 7).

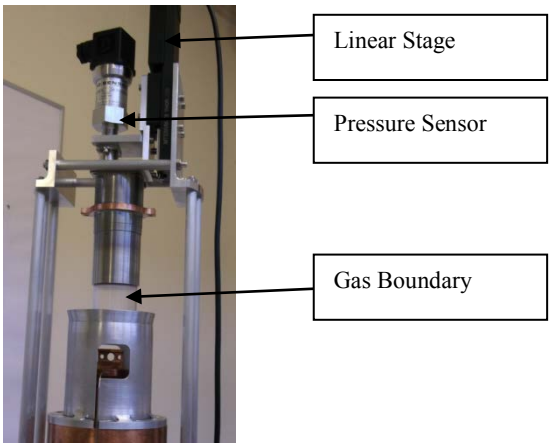

Figure 7 Gas Boundary Assembly in Open Position

The hydrogen gas is fed into the local gas boundary vessel through a path of stainless steel capillary tubes. Capillaries are used to limit the quantity of conductive material between components at room temperature the target mount. The gas is fed into the system at room temperature and through a heat exchanger, which is connected to the first stage of the pulse tube. This will pre-cool the gas to 70K so that the heat load on the second stage of the pulse tube is reduced.

The thermal radiation from the room will also provide a heat load on the pulse tube stages. Radiation shields, consisting of an Aluminium former and Multi-Layer Insulation (MLI) have been installed around the system to limit the heat load on the target end from room radiation.

Temperature and Pressure Control

The temperature control is managed using a PID controller, temperature sensors and heaters. The pressure control is managed using a PID controller, pressure sensor and a gas panel containing solenoid valves. The gas panel also contains valves that are used as part of the safety system to ensure that the hydrogen can only be fed into the system if the conditions are correct.

Target Foils

The condensation method relies on the condensed liquid flowing across a hole in the target foil and producing a liquid target film by surface tension. In order to promote the flow and surface required, a number of target foil hole profiles have been designed (figure 9).

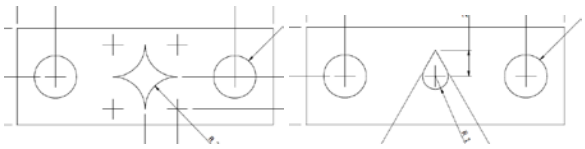

Figure 9 Target Foil Drawings

These foils have been photo-etched in copper and have a smallest feature accuracy of ±25µm. A testing program will be conducted to establish the optimum profile for efficiently producing a target of the desired parameters and will investigate the effect of inherent surface roughness that is produced by chemical etching of components and the effect of the smallest feature size as well as the geometry of the parts.

Conclusions

The mechanical and electrical assembly is complete and the system is now under engineering test to ensure that the system reaches the required temperatures and pressures prior to using hydrogen. It will also test the safety control system.

The next stage will be to determine the optimum temperature and pressure profiles to efficiently and reliably produce a target of the required parameters. Once hydrogen targets are being produced, the exact thickness shall be measured using laser interferometry and/or microscopy.

Details such as how long the target takes to produce, how long it lasts and the consistency of target formation will be available after this testing.

Acknowledgements

The author would like to thank Tom Bradshaw, Mike Courthold and Chris Pulker of STFC Technology Department for their advice during the design phase of this project.

References

1. **Preparation of solid hydrogen targets for laser fusion research;** A.N. Markov, A.B. Fradkov and V.D. Chernetskii; Kvantovaya Elektron. (Moscow) 4, 1132-1134 (May 1977)
2. **Windowless solid hydrogen target;** S. Ishimoto, T.Kobayashi, K Morimoto, I.Nomura, A.Ozawa, S. Suzuki, Y. Takahashi, I. Tanihata, T .Tsuru; Nuclear Instruments and Methods in Physics Research A 480 (2002) 304-314
3. **Production of thin solid-hydrogen foils for use as targets in high vacuum;** R. Sigel, H. Krause, S Witowski; Journal of Scientific Instruments (Journal of Physics E) 1969 Series 2 Volume 2A reference
4. **Primitive Phase Diagram for Hydrogen;** W. B. Leung and N. H. March H. Motz, Physics Letters 56A, 6 (1976), pp. 425-426